Defective gp130-mediated Signal Transducer and Activator of Transcription (STAT) Signaling Results in Degenerative Joint Disease, Gastrointestinal Ulceration, and Failure of Uterine Implantation

Matthias Ernst,[1] Melissa Inglese,[1] Paul Waring,[3] Ian K. Campbell,[2] Shisan Bao,[4] Fiona J. Clay,[1] Warren S. Alexander,[2] Ian P. Wicks,[2] David M. Tarlinton,[2] Ulrike Novak,[5] Joan K. Heath,[1] and Ashley R. Dunn[1]

[1]*Ludwig Institute for Cancer Research and* [2]*The Walter and Eliza Hall Institute, PO Royal Melbourne Hospital, VIC 3050, Australia*
[3]*Department of Pathology, Peter MacCallum Institute, East Melbourne VIC 3002, Australia*
[4]*Department of Pathology, University of Sydney, Sydney, NSW 2006, Australia*
[5]*Department of Surgery, The University of Melbourne Parkville, VIC 3052, Australia*

Abstract

The receptor subunit gp130 transduces multiple cell type–specific activities of the leukemia inhibitory factor (LIF)/interleukin (IL)-6 family of cytokines through the signal transducer and activator of transcription (STAT) and src homology 2 domain–bearing protein tyrosine phosphatase (SHP)-2/ras/Erk pathways. To define STAT-dependent physiological responses, we generated mice with a COOH-terminal gp130$^{\Delta STAT}$ "knock-in" mutation which deleted all STAT-binding sites. gp130$^{\Delta STAT}$ mice phenocopyed mice deficient for IL-6 (impaired humoral and mucosal immune and hepatic acute phase responses) and LIF (failure of blastocyst implantation). However, unlike mice with null mutations in any of the components in the gp130 signaling pathway, gp130$^{\Delta STAT}$ mice also displayed gastrointestinal ulceration and a severe joint disease with features of chronic synovitis, cartilaginous metaplasia, and degradation of the articular cartilage. Mitogenic hyperresponsiveness of synovial cells to the LIF/IL-6 family of cytokines was caused by sustained gp130-mediated SHP-2/ras/Erk activation due to impaired STAT-mediated induction of suppressor of cytokine signaling (SOCS) proteins which normally limits gp130 signaling. Therefore, the joint pathology in gp130$^{\Delta STAT}$ mice is likely to arise from the disturbance of the otherwise balanced activation of the SHP-2/ras/Erk and STAT signaling cascades emanating from gp130.

Key words: infertility • signal transduction • STAT • interleukin • gene targeting

Introduction

The activities of a family of cytokines that comprises IL-6, IL-11, leukemia inhibitory factor (LIF),* oncostatin M (OsM), ciliary neurotrophic factor (CNTF), and cardiotrophin-1 are mediated by the common signal transducing receptor β chain gp130 (1, 2). LIF/IL-6 cytokines exert multiple activities on target organs such as liver, heart, immune, hematopoietic, and nervous systems that are pivotal during embryogenesis, morphogenesis, and inflammation. Aberrant expression of LIF/IL-6 family cytokines has been associated with autoimmune disease, septic shock, and neoplasia (2, 3). Somewhat surprisingly, mice with engineered null mutations for individual LIF/IL-6 family ligands or receptor α subunits develop normally and exhibit rather mild phenotypes. IL-6–deficient (IL-6$^{-/-}$) mice, for instance, showed impaired acute phase protein production and decreased high affinity immune responses

This work was presented in part at the Mouse Molecular Genetics Meeting in Heidelberg, Germany on September 1–5, 1999.

Address correspondence to M. Ernst, Ludwig Institute for Cancer Research, PO Royal Melbourne Hospital, VIC 3050, Australia. Phone: 61-3-3941-3149; Fax: 61-3-9341-3191; E-mail: matthias.ernst@ludwig.edu.au

*Abbreviations used in this paper: CIS, cytokine-inducible src homology 2 protein; CNTF, ciliary neurotrophic factor; ES, embryonic stem; LIF, leukemia inhibitory factor; MAPK, mitogen-activated protein kinase; OsM, oncostatin M; SHP, src homology 2 domain–bearing protein tyrosine phosphatase; SOCS, suppressor of cytokine signaling; STAT, signal transducer and activator of transcription; wt, wild-type.

(4, 5), while mice deficient for LIF or the IL-11 receptor α subunit (IL-11Rα1) were unable to support pregnancies due to defective blastocyst implantation (6, 7) and decidua formation (8, 9), respectively. This finding has been attributed to partial functional redundancy between family members due to overlapping expression patterns and the sharing of common receptor β chains. Predictably, receptor β chain deficiency resulted in more severe and global effects. Depending on the genetic background, gp130$^{-/-}$ mice died in utero or shortly after birth due to myocardial hypoplasia and reduced hemopoiesis in the fetal liver (11, 12), while the LIF receptor β chain (LIF-Rβ)$^{-/-}$ mice died perinatally due to degeneration of motor neurons and astrocytes (10).

The LIF/IL-6 family of cytokines recruits gp130 according to two principal mechanisms. In the case of IL-6 and IL-11, signaling is initiated by binding to ligand-specific receptor α subunits followed by recruitment and homodimerization of two gp130 receptor β chains. In contrast, binding of LIF, OsM, CNTF, or cardiotrophin-1 induces the formation of β chain heterodimers consisting of gp130 and one of the structurally and functionally related β chains, either the LIF-Rβ or OsM receptor (1, 2). Thus, IL-6 and IL-11 are totally dependent on gp130 for signal transduction, while signals emanating from LIF, OsM, CNTF, and cardiotrophin-1 may be transduced, at least in part, by LIF-Rβ or OsM receptor. The cytoplasmic domains of all three β chains are characterized by conserved modular structures with each module thought to connect to a particular signal transduction pathway. First, the membrane-proximal homology region associates with cytoplasmic Jak kinases, which, upon receptor dimerization, phosphorylate tyrosine (Y) residues within the β chains (1). Second, a YxxV-phosphotyrosine motif (where Y is followed by any two amino acids and valine [V]) at positions Y_{757} and Y_{769} in mouse gp130 (13) and LIF-Rβ (14), respectively, is required for recruitment of the phosphatase src homology 2 domain–bearing protein tyrosine phosphatase (SHP)-2, subsequent activation of the Erk mitogen-activated protein kinase (MAPK) and transduction of mitogenic signals (15). Third, the membrane distal portion of the β chains, which contain several YxxQ-phosphotyrosine motifs, with a glutamine (Q) in position +3 relative to $Y_{765/812/904/914}$ of mouse gp130 and $Y_{976/996/1,023}$ of mouse LIF-Rβ, mediates binding and activation of the latent transcription factors signal transducer and activator of transcription (STAT)1 and STAT3 (16). This region, and in particular the YxxQ motifs, is necessary and sufficient to control differentiation and apoptosis of cells in vitro and to induce acute phase proteins in cultured hepatocytes (17–20). Moreover, the duration and intensity of the signals emanating from gp130 and LIF-Rβ appear to be limited by transcriptional induction of negative regulatory proteins of the SOCS family which impair Jak-mediated substrate phosphorylation (21, 22).

To identify the biological responses to LIF/IL-6 cytokines specifically mediated by STATs in vivo, we generated a gp130 "knock-in" mouse containing a COOH-terminal truncation mutation in gp130 (gp130$^{\Delta STAT}$) which deleted all STAT binding sites in a manner likely to be functionally equivalent to phenylalanine substitutions (Y→F) in all YxxQ motifs (17–19).

Materials and Methods

Targeting Construct and Generation of Mice. A mouse genomic 129/Sv phage library was screened with a cDNA fragment encoding the cytosolic domain of gp130, yielding a 14-kb genomic clone that contained the final two coding exons encompassing amino acids 645–671 and 672–917 (13) and a 5.4 kb of 3′ flanking sequence. PCR-mediated mutagenesis was used to introduce the gp130$^{\Delta STAT}$ truncation mutation by introducing the Y_{765}F (TAC to TTC), Q_{768}A (CAG to GCC), and V_{769}*stop* (GTC to TAG) substitutions which were encoded by the oligonucleotide 5′-TTC.AGG.CAC.GCC.TAG.G**A**C-3′. The newly introduced *stop* codon was part of an AvrII site (underlined) and was fused to the fourth nucleotide (bold A) of the 3′ untranslated region of the endogenous g130 gene. A cDNA encoding neomycin resistance preceded by an internal ribosomal entry site (IRES) was introduced into the AvrII site as a XbaI/NheI fragment, thereby generating gp130-neo dicistronic RNA. The targeting vector also contained 0.8 kb and 4.3 kb of sequence homologous to the final intron and the 3′ flanking sequence, respectively.

From 25 × 10^6 W9.5 embryonic stem (ES) cells (129/Sv) electroporated with the SalI linearized targeting construct, 12/120 neomycin resistant colonies were correctly targeted as judged by the hybridization pattern of BglII-digested DNA hybridized with a genomic fragment mapping upstream of the 5′ end of the targeting vector. Allele-specific amplification with PCR primers P1 and P2 was used to confirm the nucleotide sequence of the mutated exon in the targeted allele (see Fig. 1). Two recombinant ES cell lines (129/Sv) were injected into C57BL/6 blastocysts and the germline chimeras were mated with C57BL/6 females. Colonies homozygous for the mutation (gp130$^{\Delta STAT/\Delta STAT}$) were established and subsequently maintained by breeding gp130$^{\Delta STAT/\Delta STAT}$ males with gp130$^{\Delta STAT/wt}$ females, and their offspring were routinely genotyped at weaning age by PCR analysis using primers P1 and P2 of DNA prepared from tail biopsies.

Synovial Cell Assays. Primary cultures of synovial fibroblasts were established by sequential collagenase digestion (collagenase type II CLS-4, Worthington; 165 U/ml in DMEM) of clinically normal knee joints taken from gp130$^{\Delta STAT/\Delta STAT}$ mice and their gp130$^{wt/wt}$ littermate controls as well as compound homozygous SOCS-1$^{-/-}$, INF-γ$^{-/-}$ mice (23), and SOCS-1$^{+/+}$; INF-γ$^{-/-}$ (24) controls were established as described previously (25). Cell populations with the highest intensity of vascular cell adhesion molecule 1 staining, a marker for synovial fibroblasts (26), were maintained in DMEM supplemented with 20% FCS and assayed at passage 5.

The mitogenic activity of mouse LIF (ESGRO; AMRAD) or recombinant human IL-6 on synovial cells was assessed by culturing 2 × 10^4 cells per well in 96-well plates. After serum starvation (0.5% FCS) for 24 h, quadruplicate cultures were stimulated for 24 h with the indicated concentration of LIF or IL-6 and pulsed for the last 4 h with 0.5 μCi per well methyl-[^{3}H]thymidine (Dupont NEN) before harvesting and measuring incorporated radioactivity.

For transient transfection assays, 5 × 10^6 cells were coelectroporated (500 μFarad; 270V) with 20 μg of a luciferase reporter construct containing the MAPK responsive region (−404 to

+41) of the human c-*fos* promoter (27), 20 μg of the Srα-*β*–*galactosidase* plasmid and increasing concentrations of a Flag epitope-tagged SOCS-1 expression construct (pSOCS-1; reference 28). Cells in 24-multiwell plates were maintained in 0.5% FCS for 48 h in the presence of IL-6 plus sIL-6R (500 ng/ml each), saline, or FCS (10%) before lysis with 40 μl of reporter lysis buffer (Promega). Lysates were assayed for luciferase activity which was normalized according to the β-galactosidase activity. Expression levels from the transfected SOCS-1 plasmid were monitored by anti-Flag immunoblotting (28).

Immunoblotting and In Vitro Phosphorylation Assay. Serum-starved cultures of synovial fibroblasts were stimulated with IL-6 plus sIL-6R (both at 500 ng/ml) for the indicated period of time. 1 mg of cell lysate was immunoprecipitated with an antiserum against Jak-2 (UBI) and used for in vitro phosphorylation experiments in the presence of γ-[^{32}P]ATP as described previously (19). SHP-2 immunoprecipitates were resolved by SDS-PAGE and blots were probed with antiphosphotyrosine (UBI) and SHP-2 (Santa Cruz Biotechnology, Inc.) antibodies to assess protein loading (19). For detection of active Erk MAPK, 50 μg of total cell lysate were resolved by SDS-PAGE and transferred proteins were reacted with an antibody that recognizes phosphorylated Erk1/2 (New England Biolabs, Inc.). The level of Erk protein was subsequently visualized by reaction with anti-Erk1/2 antibodies (Santa Cruz Biotechnology, Inc.). STAT3 phosphorylation in tissues was monitored after STAT3 immunoprecipitation (Santa Cruz Biotechnology, Inc.) of 2 mg of tissue lysate obtained from mice 20 min after a single intravenous injection of either 5 μg IL-6, LIF, IL-11, or saline and detection with antiphosphotyrosine and anti-STAT3 (Transduction Laboratories) antibodies, respectively (19).

Northern Blot Analysis. Poly(A)$^+$ RNA was prepared from livers of mice 40 min (for SOCS induction) or 4 h (for acute phase protein) after a single intravenous injection of 5 μg of LIF, IL-6, or saline according to standard protocols. Poly(A)$^+$ RNA was also isolated from cultures of primary synovial cells stimulated with IL-6 plus sIL-6R (both at 500 ng/ml) for 45 and 180 min, respectively. 3 μg of poly(A)$^+$ RNA were hybridized with cDNAs encoding either cytokine-inducible src homology 2 protein (CIS), SOCS-1, SOCS-2, or SOCS-3, gp130 or neomycin, and serum amyloid A or haptoglobin. All RNA blots were finally hybridized for glyceraldehyde 3-phosphate dehydrogenase (GAPDH) to assess the amounts of RNA analyzed.

Clinical Assessment and Histology. For each limb, clinical scores were allocated for erythema, swelling, and flexibility of joints twice per week for up to 25 wk as described previously (29). The scoring system for each limb was as follows: 0, normal; 1, moderately affected; and 2, severely affected. Soft tissues were fixed in formalin for 24 h, while joints were fixed in 10% formalin for 48 h, decalcified, and embedded in paraffin (29). Sections were stained with hematoxylin and eosin. Histopathological features associated with the large appendicular joints (shoulder, elbow, wrist, hip, knee, ankle) were scored as 0, normal; 1, minor synovial changes without degenerative alterations or cartilage metaplasia; 2, mild degenerative joint disease with cartilage deposits with or without synovial hyperplasia; and 3, severe degenerative joint disease with marked cartilage metaplasia with or

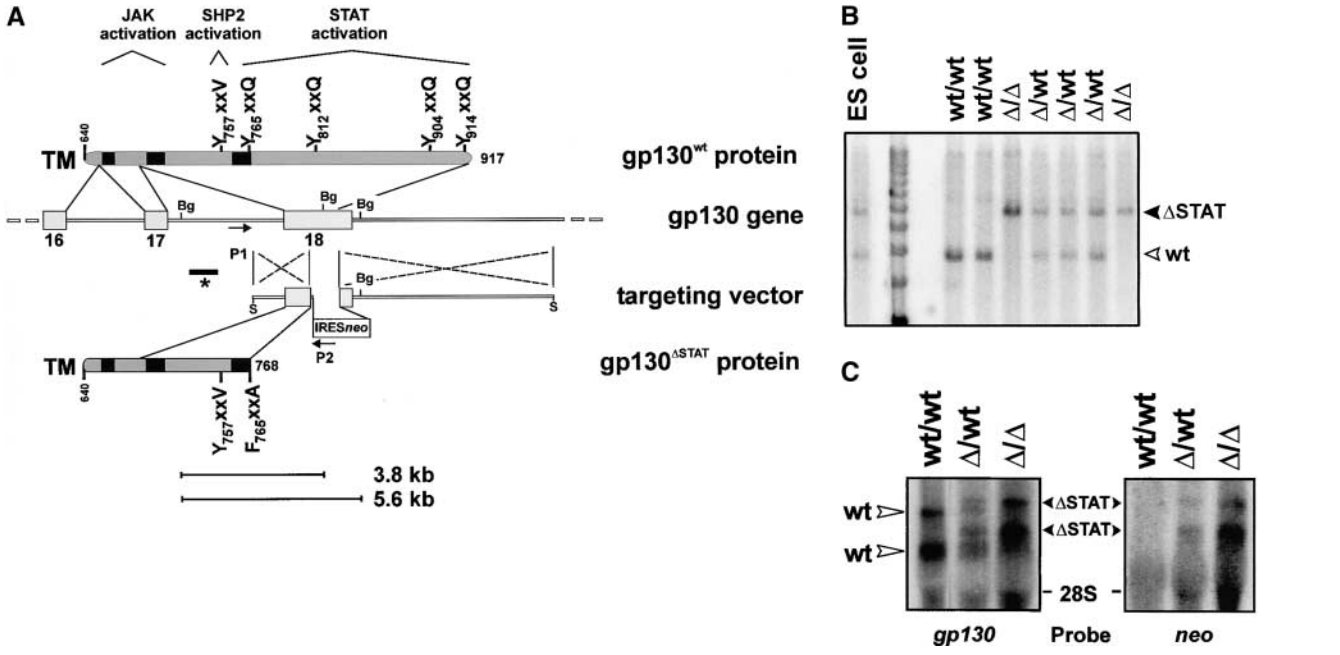

Figure 1. Generation of gp130$^{\Delta STAT/\Delta STAT}$ mice. (A) Targeting strategy for the introduction of the gp130$^{\Delta STAT}$ truncation. The cytoplasmic domain of mouse gp130 with its homology motifs Box1, Box2, and Box3 (black) are schematically depicted alongside the corresponding genomic structure with exons numbered according to Betz et al. (reference 31). The targeting vector contains a $Y_{765}RHQ_{768}$ to FRHA substitution and a translational *stop* codon at position 769 preceding a ribosomal reentry site and the sequence encoding neomycin resistance (IRES*neo*). A diagnostic digest with BglII (Bg) yields a fragment of 3.8 kb from the wt allele and a 5.6-kb fragment from the targeted allele when hybridized with a probe external to the targeting vector (*). P1 and P2 refer to primers used for an allele-specific PCR reaction. S, SalI. (B) Southern blot analysis of BglII digests of DNA prepared from a targeted ES cell line and tail biopsies obtained from offspring of gp130$^{\Delta STAT/wt}$ intercrosses. The immobilized DNA was hybridized with a probe (* in A) external to the targeting construct. (C) Northern blot analysis of liver RNA extracted from offspring of gp130$^{\Delta STAT/wt}$ matings. Poly(A)$^+$ RNA was hybridized with a cDNA fragment encoding the extracellular portion of gp130. Dicistronic gp130$^{\Delta STAT}$-neo mRNA transcripts were ~1.4 kb larger than the two major wt gp130 mRNA species. The same blot was stripped and reprobed for expression of the *neo* gene.

without synovial hyperplasia. All clinical and histological assessments were performed blind.

Immunization, ELISA, and Immunohistochemistry. Mice were immunized by injecting ~1 μl of OVA, (1 mg/ml in PBS, pH 7.4, emulsified with Freund's Complete Adjuvant) into each Peyer's patch (30). Mice were boosted intraduodenally 14 d later with OVA and euthanized 5 d after the secondary challenge. The proteinacious fraction of fecal pellets, obtained from intestinal washes, was prepared as described previously (30) and the small intestine was collected, fixed in cold ethanol, embedded in paraffin, and sectioned (5 μm) for immunohistochemistry of OVA-containing cells (5). OVA-specific ELISA assays were carried out for IgA, IgG, and IgM using Ig-specific biotin conjugated goat anti–mouse antibodies (Zymed Laboratories). Total isotype-specific Ig levels in sera of unchallenged mice were determined by ELISA using commercially available kits according to the manufacturer's recommendations (Bethyl Laboratories, Inc.).

Embryo Cross-Fostering. Blastocysts were flushed from uteri on day 4 of gestation (day 1 is day of plug) and transferred to day 3 pseudopregnant recipients as described previously (6). All offspring were genotyped by Southern blotting of DNA from tail biopsies.

Results

To inactivate the four YxxQ STAT-binding sites in gp130 at positions $Y_{765/812/904/914}$, we replaced exon 18, encoding amino acids 672–917, with a version truncated at the COOH-terminal side of amino acid 768 and containing the $Y_{765}F$ and $Q_{768}A$ substitutions. After homologous recombination in ES cells, the presence of the expected mutations was confirmed by sequencing allele-specific PCR amplicons generated from the targeted gp130 allele with primers P1 and P2 (Fig. 1 A). Transcription of the mutated gp130 allele generated a dicistronic gp130-neo mRNA species ~1.4 kb larger than wild-type (wt) gp130 mRNA which encoded a truncated $gp130^{\Delta STAT}$ protein (Fig. 1 C). Interbreeding of $gp130^{\Delta STAT/wt}$ mice yielded homozygous offspring close to the expected Mendelian ratio (Fig. 1 B and Table I). However, subsequent matings of $gp130^{\Delta STAT/wt}$ females with $gp130^{\Delta STAT/\Delta STAT}$ males yielded significantly fewer $gp130^{\Delta STAT/\Delta STAT}$ than $gp130^{\Delta STAT/wt}$ offspring at weaning age (Table I), although mice of the two genotypes were recovered at equal ratios during embryonic development (E18, and data not shown). At birth, $gp130^{\Delta STAT/\Delta STAT}$ mice appeared superficially healthy, but in comparison to $gp130^{wt/wt}$ and $gp130^{\Delta STAT/wt}$ littermates, they showed a 20–30% reduction in body weight (1.93 g ± 0.38 g vs. 2.93 g ± 0.12 g; $P < 0.05$, $n = 20$) and trunk length, which persisted throughout adulthood. The average life span of $gp130^{\Delta STAT/\Delta STAT}$ mice was reduced (6 ± 1 mo for males, 8 ± 2 mo for females) compared with $gp130^{\Delta STAT/wt}$ littermates (15 ± 2 mo for both sexes) which were indistinguishable from $gp130^{wt/wt}$ mice in all aspects analyzed.

Table I. *Reproductive Frequency in gp130 Mutant Mice*

Male[a]	Female	Live pups
wt/Δ (17)	wt/Δ (17)	wt/wt (66)
		wt/Δ (156)
		Δ/Δ (57)
Δ/Δ (47)	wt/Δ (47)	wt/Δ (328)[b]
		Δ/Δ (179)[b, c]
wt/Δ (15)	Δ/Δ (6)	wt/Δ (0)
		Δ/Δ (0)
Δ/Δ (8)	Δ/Δ (3)	Δ/Δ (0)

Male[d]	Female	Numbers of blastocysts transferred	Foster mother	Live pups
wt/Δ	Δ/Δ (2)	28	wt/wt (2)	wt/Δ (4)
				Δ/Δ (5)
wt/Δ	wt/wt (5)	28	Δ/Δ (3)	wt/wt (0)
				wt/Δ (0)
wt/Δ	wt/wt (5)	29	wt/wt (3)	wt/wt (5)
				wt/Δ (3)

[a]Test breeding of gp130 mice of the indicated genotypes. All parents and offspring were genotyped by PCR analysis of DNA from tail biopsies. Each $gp130^{\Delta STAT/\Delta STAT}$ female was test mated at least twice with a male of proven fertility. Number of animals is indicated in parentheses.
[b]67 pups in total were cannibalized by their mothers before genotyping.
[c]$P < 0.001$ when compared with the expected 1:1 ratio between genotypes (chi-squared analysis).
[d]Transfer of blastocysts into pseudopregnant recipient mice. Blastocysts were flushed from the uteri on day 4 of gestation and transferred to day 3 pseudopregnant recipients. Numbers of animals in indicated in parentheses.
Δ/Δ, Δ/wt, and wt/wt refers to $gp130^{\Delta STAT/\Delta STAT}$, $gp130^{\Delta STAT/wt}$, and $gp130^{wt/wt}$ mice, respectively.

Failure of Uterine Implantation and Hepatic Acute Phase Response. While gp130$^{\Delta STAT/\Delta STAT}$ male mice sired litters of equal size to those of gp130$^{\Delta STAT/wt}$ or wt males, female gp130$^{\Delta STAT/\Delta STAT}$ mice mated with males of any genotype showed no external signs of pregnancy (Table I). Histological analysis of uteri from gp130$^{\Delta STAT/\Delta STAT}$ mice 5.5 d after coitum revealed the presence of blastocysts that showed no overt signs of implantation at a time when embryos in uteri of gp130$^{\Delta STAT/wt}$ and gp130$^{wt/wt}$ mice had implanted and were surrounded by the secondary decidua (Fig. 2 A). However, blastocysts of all genotypes recovered from gp130$^{\Delta STAT/\Delta STAT}$ mice developed to term when surgically transferred to day 3 pseudopregnant wt recipient mice, while again no signs of pregnancy were observed when transferred to gp130$^{\Delta STAT/\Delta STAT}$ recipient mice (Table I). These results unequivocally show a maternal defect at the time of embryo implantation that is strikingly similar to the defect described in mice deficient for LIF (6, 7).

To determine whether impaired STAT signaling in the uteri of gp130$^{\Delta STAT/\Delta STAT}$ mice was the likely reason for the failure of blastocyst implantation and subsequent decidua formation, we monitored STAT3 phosphorylation in the liver and uterus after single bolus injections of IL-6, IL-11, or LIF. In both tissues, STAT3 phosphorylation in gp130$^{\Delta STAT/\Delta STAT}$ mice was markedly reduced in response to LIF and completely abrogated in response to IL-6 or IL-11, compared with identically treated heterozygous control mice (Fig. 2, B and D). This observation was further pursued in liver by measuring the induction of hepatic class I acute phase genes which are regarded as classical STAT-mediated responses (20). Induction of serum amyloid A and haptoglobin mRNAs in gp130$^{\Delta STAT/\Delta STAT}$ mice was

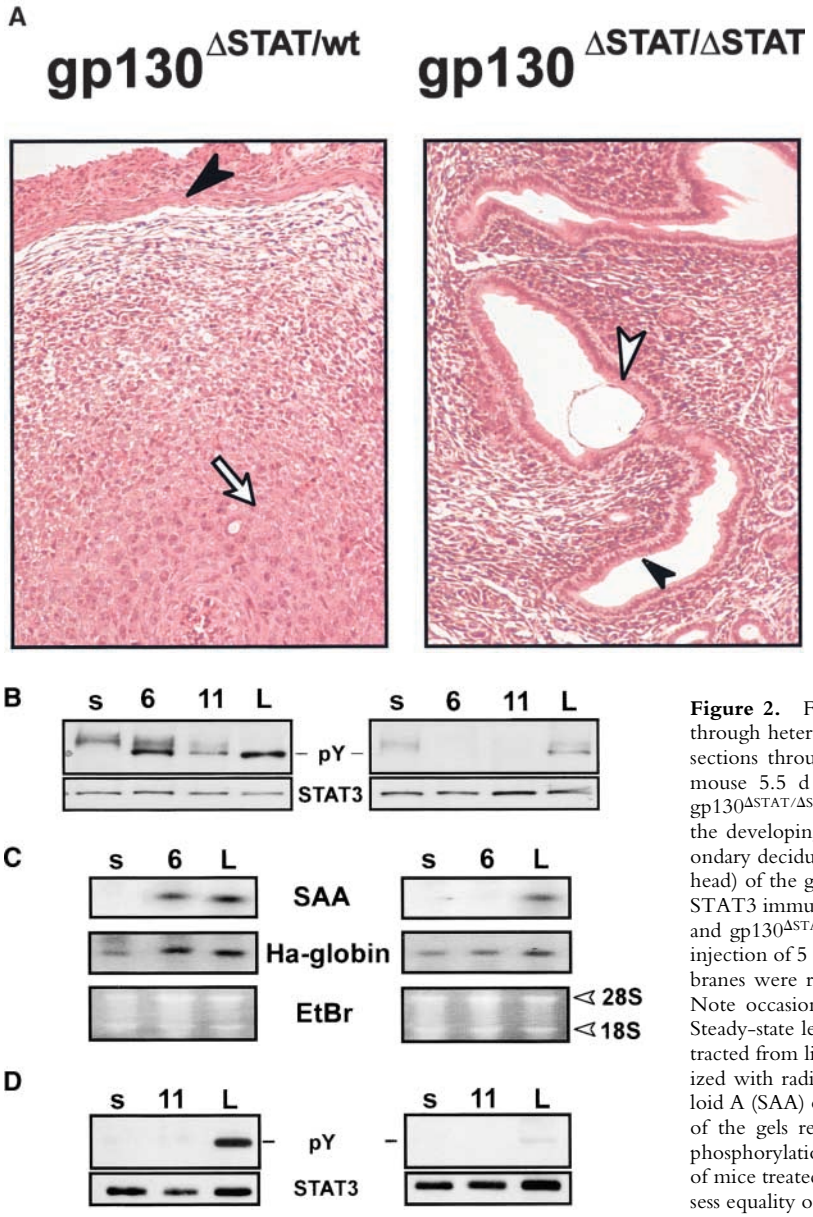

Figure 2. Failure of blastocyst implantation due to impaired signaling through heterodimeric gp130$^{\Delta STAT}$/LIF-Rβ complexes. (A) Histological sections through the uteri from a gp130$^{\Delta STAT/wt}$ and gp130$^{\Delta STAT/\Delta STAT}$ mouse 5.5 d after coitum. The blastocyst (white arrowhead) in the gp130$^{\Delta STAT/\Delta STAT}$ uterus showed no signs of implantation. In contrast, the developing embryo is surrounded by stromal cells forming the secondary decidua (white arrow) beneath the epithelial lining (black arrowhead) of the gp130$^{\Delta STAT/wt}$ uterus. (B) Tyrosine phosphorylation (pY) of STAT3 immunoprecipitates prepared from liver of gp130$^{\Delta STAT/wt}$ control and gp130$^{\Delta STAT/\Delta STAT}$ mutant mice 20 min after a single intraperitoneal injection of 5 μg of IL-6 (6), IL-11 (11), LIF (L), or saline (s). The membranes were reprobed for STAT3 to assess equality of protein loading. Note occasional appearance of a nonspecific band above STAT3. (C) Steady-state levels of mRNA for hepatic type I acute phase proteins extracted from livers of mice as in B. 3 μg of poly(A)$^+$ RNA were hybridized with radiolabeled full length cDNAs encoding human serum amyloid A (SAA) or haptoglobin (Ha-globin). Ethidium bromide (EtBr) stain of the gels revealed similar amounts of RNA analyzed. (D) Tyrosine phosphorylation (pY) of STAT3 immunoprecipitates prepared from uteri of mice treated as in B. The membranes were reprobed for STAT3 to assess equality of protein loading.

clearly diminished in response to LIF and absent in response to IL-6 (Fig. 2 C). Collectively, these results suggest that the mutant receptor β chain heterodimers between gp130$^{\Delta STAT}$ and LIF-Rβ (which retains the 3 YxxQ motifs in LIF-Rβ) induced by LIF, while less efficient than a wt gp130/LIF-Rβ complex containing 7 YxxQ motifs, retains some STAT-mediated signaling capacity. Meanwhile homodimers formed between two truncated gp130$^{\Delta STAT}$ proteins in response to IL-6 and IL-11 failed to promote STAT-mediated signaling.

Gastrointestinal Ulceration and Impaired Humoral and Mucosal Immunity. Under specific pathogen–free conditions, approximately half of all gp130$^{\Delta STAT/\Delta STAT}$ mice of 4 mo of age showed occult traces of fecal blood and ulceration of the gastric pylorus (Fig. 3 a). We also observed ulceration of the anorectal region which was invariably associated with rectal prolapse. Notably, the ulceration at both sites was confined to the vicinity of the sphincters suggesting defective epithelial repair in response to sustained mucosal injury. Mutant mice kept under conventional conditions also developed caecal ulcers (41%; Fig. 3 b) and acute inflammation at additional mucosal sites including the conjunctivae (41%) and the nasolacrimal ducts (29%). Furthermore, in comparison to gp130$^{\Delta STAT/wt}$ mice, gp130$^{\Delta STAT/\Delta STAT}$ mice showed a much higher load of *Giardia muris* which is an endemic parasite in the conventional facility in which the mice were housed.

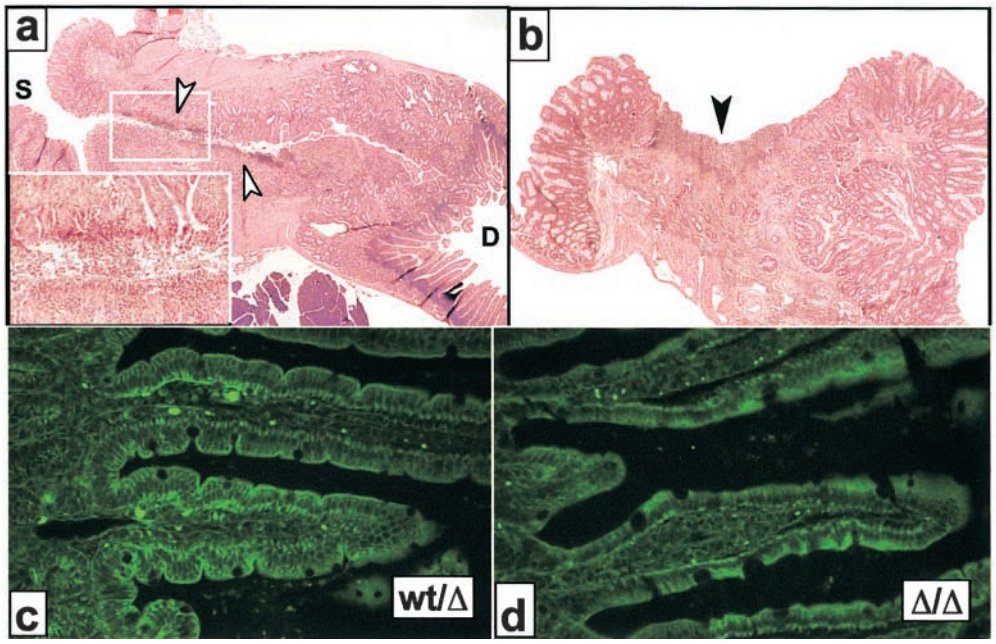

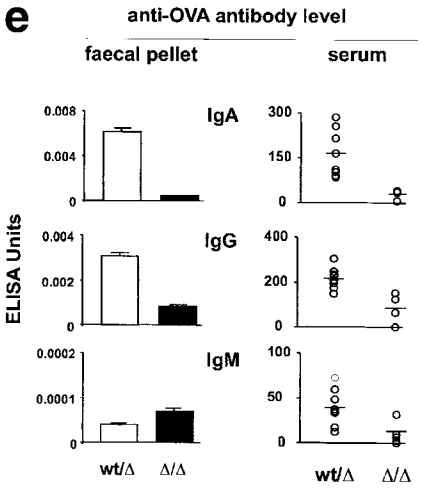

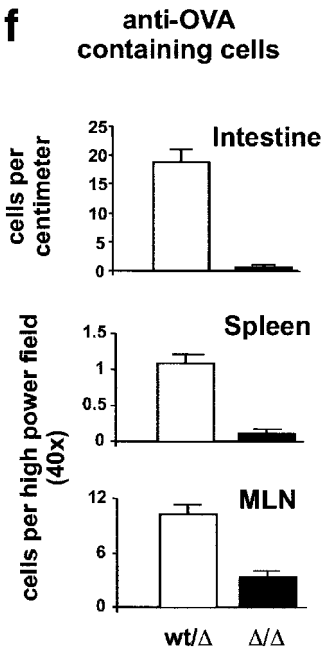

Figure 3. Gastrointestinal ulceration and impaired immunity in gp130$^{\Delta STAT/\Delta STAT}$ mice. Mucosal ulcers (arrowheads) in the gastric pylorius (a) and caecum (b). High magnification (insert) shows surface ulcer debris, neutrophil-rich inflammatory exudates, and regenerative changes in adjacent epithelial cells. S, stomach; D, duodenum. (c and d) Appearance of OVA-containing plasma cells in the lamina propria of small intestinal villi in gp130$^{\Delta STAT/wt}$ control (c) and gp130$^{\Delta STAT/\Delta STAT}$ mutant (d) mice detected by FITC-mediated immunofluorescence of anti-OVA antibodies. (e) Isotype-specific anti-OVA antibody response in extracts of fecal pellets and serum of gp130$^{\Delta STAT/\Delta STAT}$ mutant and gp130$^{\Delta STAT/wt}$ control mice. Mice were immunized by injection of OVA directly into Peyer's patches and boosted with OVA 14 d later. OVA-specific Ig levels were determined after a further 5 d as described in Materials and Methods. Mean ± SEM, $n = 7$. (f) Number of OVA-specific plasma cells in the small intestine, spleen, and mesenteric lymph nodes (MLN) of mice used for the experiment in Fig. 2 E. Data were obtained by immunofluorescent histology with FITC-conjugated goat–anti mouse heavy chain reagent and represent the mean ± SEM in 30–50 randomly selected high power fields per mouse with four mice per group.

Since IL-6 is required for differentiation of B cells to high affinity IgA- and IgG-producing plasma cells (4, 5, 31), we sought to determine mucosal immune responses of $gp130^{\Delta STAT/\Delta STAT}$ mice. In the absence of deliberate immunization and compared with heterozygous controls, mutant mice showed reduced levels of circulating IgA ($gp130^{\Delta STAT/\Delta STAT}$, 0.62 ± 0.05 mg/ml, $n = 7$ vs. $gp130^{\Delta STAT/wt}$ mice, 0.85 ± 0.10 mg/ml, $n = 6$), IgG_1 (0.17 ± 0.07 mg/ml vs. 0.35 ± 0.11 mg/ml), IgG_{2a} (0.18 ± 0.13 mg/ml vs. 0.53 ± 0.12 mg/ml), and IgG_{2b} (0.38 ± 0.15 mg/ml vs. 0.87 ± 0.17 mg/ml). In contrast, the levels of circulating IgM were similar for mice of both genotypes. The capacity of $gp130^{\Delta STAT/\Delta STAT}$ mice to mount a specific intestinal IgA response after local immunization of Peyer's patches with OVA was grossly impaired when assessed by OVA-specific Ig isotype level in fecal pellets and serum (Fig. 3 e). Similarly, the OVA-specific IgG response in the intestine was also reduced and there were significantly less anti-OVA–containing cells in the small intestine (Fig. 3, c and d), mesenteric lymph nodes, and spleen of $gp130^{\Delta STAT/\Delta STAT}$ mice (Fig.3 f) reminiscent of the findings reported previously in IL-6–deficient mice (30). Collectively, these data imply that gp130 transduces the IL-6–mediated final maturation of B cells to high affinity Ig-secreting plasma cells via its STAT-binding sites in the COOH-terminal domain.

Severe Degenerative Joint Disease in $gp130^{\Delta STAT/\Delta STAT}$ Mice. Unexpectedly, swelling of one or more of the large weight-bearing joints was observed in 60% of adult $gp130^{\Delta STAT/\Delta STAT}$ mice ($n = 49$, mean age 89 d ranging from 56–412 d), which resulted in flexion deformities of the hind limbs and reluctance of the mice to stand (Fig. 4, a and b). Joints of $gp130^{\Delta STAT/\Delta STAT}$ mice were often affected bilaterally but only rarely showed signs of erythema. Systematic clinical assessment showed that all $gp130^{\Delta STAT/\Delta STAT}$ mice showed stiffness of one or more limbs with restricted flexion and extension of the ankles as well as dorsiflexion at the wrist joints (Fig. 4 b to e). Notably, some degree of joint restriction was already evident in one or more limbs of P7-neonatal $gp130^{\Delta STAT/\Delta STAT}$ mice but did not increase significantly with age and only rarely affected previously healthy joints (Table II). By contrast, none of the $gp130^{\Delta STAT/wt}$ control mice showed any clinical evidence

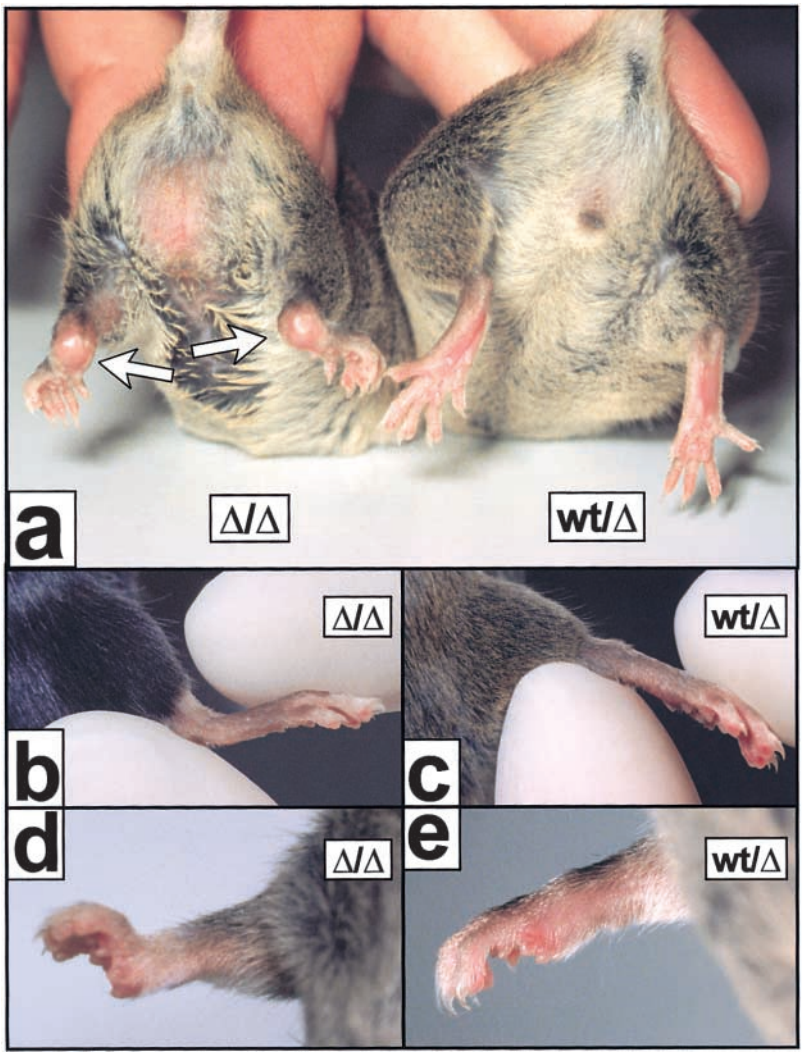

Figure 4. Clinical assessment of the joint disease in $gp130^{\Delta STAT/\Delta STAT}$ mice. Swollen ankle joints and characteristic flexion deformities of hind legs in bilaterally affected $gp130^{\Delta STAT/\Delta STAT}$ mice (a). The restriction of ankle movement (b and c) and fixed flexion deformation of front paws (d and e) were consistent findings in $gp130^{\Delta STAT/\Delta STAT}$ mice but were never seen in $gp130^{\Delta STAT/wt}$ littermates.

of swelling or restricted joint movement at any age. Abnormal joints were also observed in gp130$^{\Delta STAT/\Delta STAT}$ mice maintained under specific pathogen–free conditions, indicating that this pathology was unlikely to be secondary to infections at mucosal sites.

The joints of 49 clinically affected mice were examined histologically and graded as described in Materials and Methods. Of the 292 large appendicular joints examined (16 hips, 75 knees, 67 ankles, 40 shoulders, 50 elbows, 44 wrists), 76% were scored as 0 or 1 while 24% were graded as 2 or 3. Curiously, joints showing degenerative changes (grade 2 or 3) were twice as common in male (27.8%, n = 65) than female (15.1%, n = 8) gp130$^{\Delta STAT/\Delta STAT}$ mice. Histologically, these joints showed cartilaginous nodules along the joint capsule extending from the edge of the articular cartilage. In the knee joints, these nodules invariably replaced the menisci and supporting connective tissue (Fig. 5, a and b) and occasionally the joint spaces contained dislodged and rounded cartilaginous nodules (Fig. 5 e). These changes were often accompanied by enlargement and deformation of the joints which occasionally affected the growth plate (Fig. 5 b). In addition, joints of older gp130$^{\Delta STAT/\Delta STAT}$ mice often showed erosion of the articular surface and mild synovial hyperplasia associated with the tendon sheaths and nonswollen joints. Since histological examination of clinically affected joints of newborns revealed considerable structural variability, we were unable to unambiguously ascribe histological abnormalities to these joints. However, no primary irregularities were detected in the growth plate of young adult gp130$^{\Delta STAT/\Delta STAT}$ mice. Occasionally, marked synovial hyperplasia was observed in the recesses of the joint cavities with expansion of the subsynovial connective tissue adjacent to the articular surfaces (Fig. 5, c and d). However, foci of metaplastic cartilage were rarely observed within this de novo–formed connective tissues suggesting that the cartilaginous nodules were composed of newly formed cartilage and not disordered menisci or articular cartilage. Inflammatory cells, primarily lymphocytes and macrophages, were present in low numbers in the synovium and subsynovial tissues of pathological joints; however, neutrophils were usually absent. Collectively, these observations suggest that the joint pathology in gp130$^{\Delta STAT/\Delta STAT}$ mice was primarily a result of synovial hyperplasia with progressive chronic inflammation and secondary cartilaginous metaplasia restricting joint movement and culminating in the degeneration of the articular cartilage of the major weight-bearing joints in older mice (Fig. 5, f and g).

Enhanced Mitogenic Response of Synovial Fibroblasts to IL-6. Since the LIF/IL-6 family cytokines have been implicated in promoting synovial hyperplasia (32, 33), we investigated whether altered signaling through gp130$^{\Delta STAT}$ receptors affected the mitogenic response of mutant synovial cells

Table II. *Clinical Assessment of Joint Stiffness in gp130$^{\Delta STAT/STAT}$ Mice*

	Age (d)	30	50	71	98	141	176
	Limb						
Mouse 1	Rear left	1	1	1	1	2	2
	Rear right	1	1	1	1	1	1
	Front left	0	0	0	0	0	0
	Front right	2	2	2	2	2	2
Mouse 2	Rear left	1	1	1	1	2	2
	Rear right	1	1	1	1	1	1
	Front left	0	0	0	1	1	1
	Front right	0	0	0	1	1	1
Mouse 3	Rear left	1	1	0	1	1	2
	Rear right	1	1	1	2	1	1
	Front left	0	0	0	0	0	0
	Front right	0	0	0	0	0	0
Average score per gp130$^{\Delta STAT/STAT}$ mouse (n = 14)		3.3 ± 1.2	2.9 ± 1.7	3.0 ± 1.2	3.3 ± 1.2	3.5 ± 1	3.5 ± 1.1
Average score per gp130$^{\Delta STAT/wt}$ mouse (n = 21)		0	0	0	0	0	0

Mice were clinically assessed and scores for joint movement were allocated as described in Materials and Methods. Each limb of mice in cohorts of gp130$^{\Delta STAT/\Delta STAT}$ and gp130$^{\Delta STAT/wt}$ animals was assessed twice per week for restriction in wrist and ankle movement as illustrated in Fig. 4 c to f. Scores were allocated for: 0, no restriction; 1, moderate restriction; and 2, severe restriction, with 8 being the maximal score per mouse. None of the gp130$^{\Delta STAT/wt}$ control mice scored positive at any time point. The table shows the results for selected time points of three representative gp130$^{\Delta STAT/\Delta STAT}$ mice and the average score per mouse in the mutant cohort (mean ± SD, n = 14).

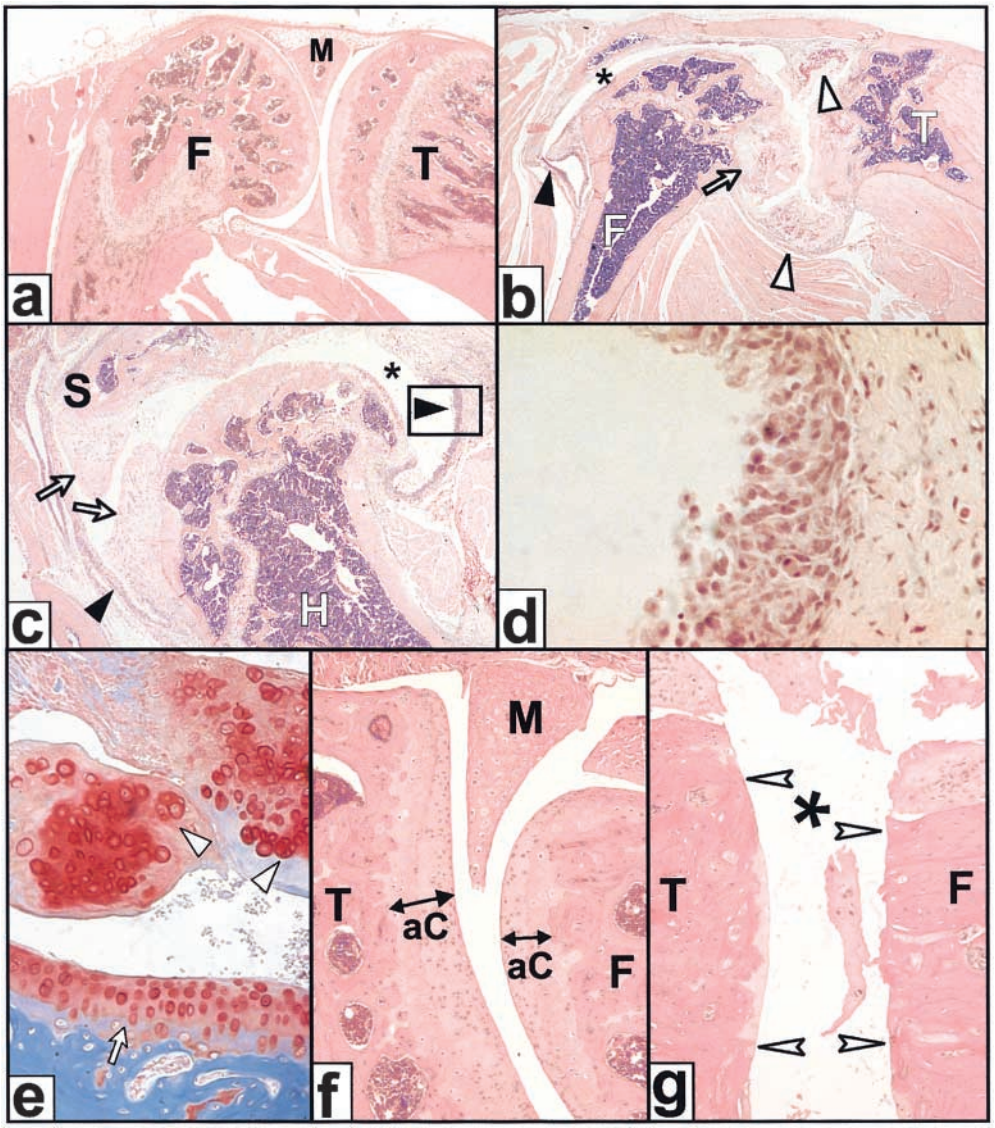

Figure 5. Histological assessment of joint disease in gp130$^{\Delta STAT/\Delta STAT}$ mice. Sagittal sections of knees of age-matched 71-d-old gp130$^{\Delta STAT/wt}$ control (a) and gp130$^{\Delta STAT/\Delta STAT}$ mutant mice (b). The section of the mutant knee shows enlargement of the synovial space (*), synovial hyperplasia and pannus formation (black arrowhead), cartilaginous overgrowth in the menicsi (white arrowhead), and destruction and deformation of the articular surfaces. Note that the cartilaginous metaplasia on the head of the femur (arrow) is associated with alterations of the growth plate. The shoulder (c) joint of gp130$^{\Delta STAT/\Delta STAT}$ mouse illustrates the early stage manifested as enlargement of the synovial space (*), prominent synovial hyperplasia (arrowheads), exuberant pannus formation with early cartilaginous metaplasia (arrows) but little destruction of the articular surface. A high magnification (d) of the area boxed in c shows synovial hyperplasia in the recess of the cavity of the shoulder joint. The metaplastic cartilage deposits within the synovial cavity (e) contain disorganized clusters of chondrocytes (arrowhead) which occupy lacunae within the matrix and contrast the organized appearance of smaller chondrocytes in "columns" in normal articular cartilage (arrow); Safranin-O and Alcian Blue stain proteoglycan red and mineralized matrix blue, respectively. Frontal sections through knees from 180-d-old gp130$^{\Delta/wt}$ (f) and gp130$^{\Delta/\Delta}$ mice (g) document the expanded synovial space (*), destruction, and erosion of the articular cartilage (aC arrowhead). aC, articular cartilage; F, femur; H, humerus; M, meniscus; S, scapula; T, tibia.

in vitro. Primary cultures of synovial fibroblasts, derived from clinically unaffected knees of gp130$^{\Delta STAT/\Delta STAT}$ mice, showed an enhanced rate of [^{3}H]thymidine incorporation in response to IL-6 or LIF when compared with cells obtained from gp130$^{wt/wt}$ mice (Fig. 6 A). Furthermore, mutant cells responded to 100- to 1,000-fold lower concentrations of cytokines than wt cells and showed sustained IL-6–dependent activation of gp130-mediated signaling, as demonstrated by autophosphorylation of Jak-2, tyrosine phosphorylation of SHP-2, and phosphorylation of MAPK isoforms Erk1/2 (Fig. 6 B). These in vitro data indicate increased sensitivity and proliferative response of mutant synovial fibroblasts to IL-6 associated with sustained gp130 signaling through the SHP-2/ras/Erk pathway.

Sustained Activation of the SHP-2/ras/Erk Pathway Results from Impaired Induction of SOCS-1. One possible mechanism accounting for sustained activation of the SHP-2/ras/Erk pathway in response to IL-6 could be that impaired STAT activation retarded the termination of gp130-mediated signaling. We hypothesized that this might result from impaired induction of SOCS/CIS family gene expression (21, 22). As depicted in Fig. 7 A, the expression of CIS, SOCS-1, SOCS-2, and SOCS-3 mRNA were readily induced in the livers of wt mice after a single injection of either IL-6 or LIF. IL-6 treatment also induced CIS and SOCS-2 mRNA in the livers of gp130$^{\Delta STAT/\Delta STAT}$ mice, however, we observed almost complete absence of SOCS-1 mRNA induction and re-

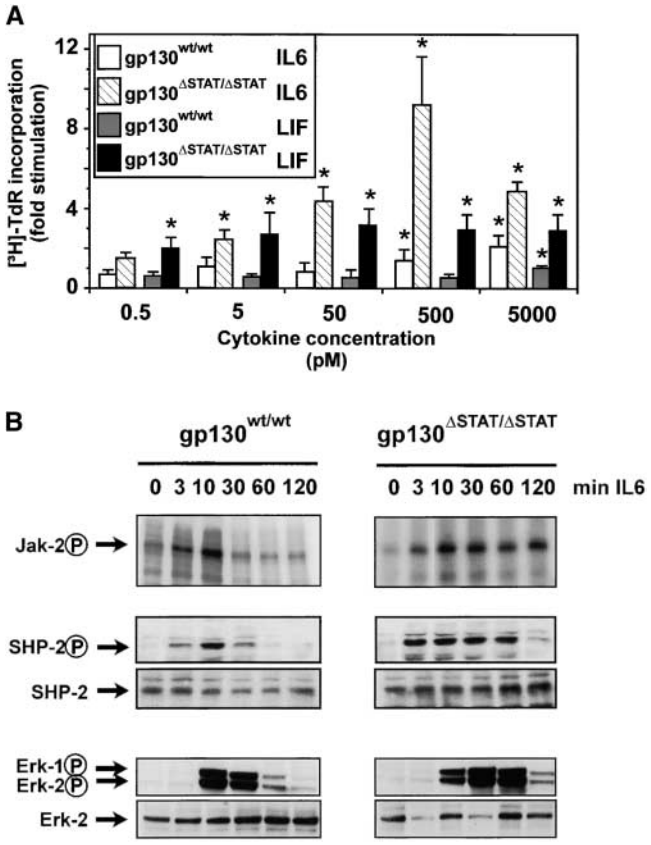

Figure 6. Hyperresponsiveness of synovial cells correlates with sustained Erk MAPK activation. (A) [^{3}H]thymidine incorporation by synovial cells prepared from wt and gp130$^{\Delta STAT/\Delta STAT}$ mice and stimulated with LIF or IL-6. Cells derived from clinically unaffected joints were stimulated for 24 h with the indicated concentration of LIF or IL-6 in the presence of sIL-6R (500 ng/ml). Each point represents the mean ± SD. $^*P < 0.05$ compared with unstimulated cultures of the same genotype. (B) Activation of intermediate signaling molecules in synovial cells stimulated with IL-6 and sIL-6R (both at 500 ng/ml) for the indicated period of time. Cell lysates were immunoprecipitated with either a Jak-2 antiserum and incubated with γ-[^{32}P]ATP to assess Jak-2 autophosphorylation, or with a SHP-2 antiserum and blotted with antiphosphotyrosine antibodies. Erk MAPK activation was analyzed by directly probing lysates with an antibody specific for phospho-Erk1/2 (Erk-P). The total amount of SHP-2 and Erk proteins was assessed by reprobing the membranes for SHP-2 and Erk1/2, respectively.

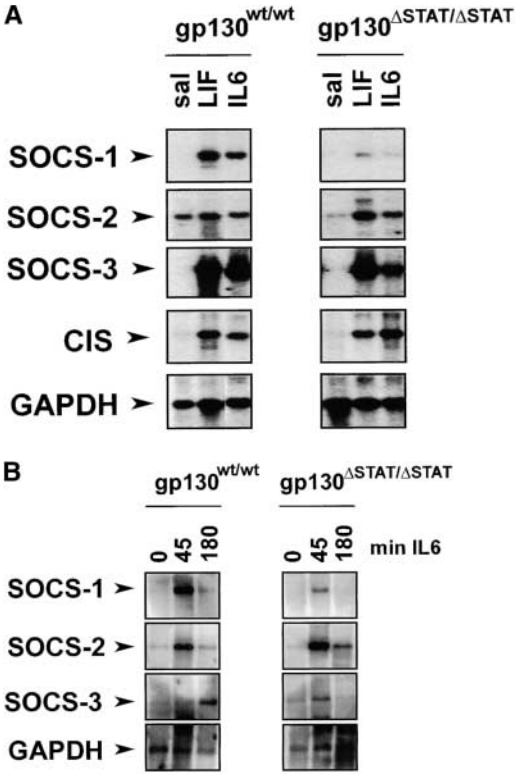

Figure 7. Impaired induction of SOCS mRNA in response to signaling through gp130$^{\Delta STAT}$. (A) SOCS/CIS mRNA steady-state levels after cytokine stimulation in vivo. Northern blot analysis of poly(A)$^+$ RNA extracted from livers of gp130$^{\Delta STAT/\Delta STAT}$ and wt mice 40 min after a single intravenous injection of 5 μg of LIF, IL-6, or saline. Blots were sequentially probed for SOCS-1, SOCS-2, SOCS-3, CIS, and finally GAPDH to assess for amounts of RNA analyzed. (B) Induction of SOCS-1 and SOCS-3 mRNA steady-state levels in synovial cells stimulated with IL-6 and sIL-6R for the indicated period of time. Northern blots analysis of poly(A)$^+$ RNA probed for SOCS-1, SOCS-3, and GAPDH to assess for amounts of RNA analyzed.

duced SOCS-3 mRNA induction. Notably, the induction of SOCS-1 mRNA was also markedly reduced in synovial cells from gp130$^{\Delta STAT/\Delta STAT}$ mice compared with cells from wt mice (Fig. 7 B). These data support previous observations suggesting that IL-6–dependent activation of SOCS-1 and SOCS-3 genes is mediated, at least in part, by STATs (34). The reduced induction of SOCS-1 mRNA observed in the livers of LIF-treated gp130$^{\Delta STAT/\Delta STAT}$ mice (Fig. 7 A) most likely resulted from diminished STAT signaling through the less effective gp130$^{\Delta STAT}$/LIF-Rβ heterodimers.

To explore the concept of enhanced gp130-mediated SHP-2/ras/Erk signaling in the absence of SOCS-1, we analyzed IL-6-signaling in SOCS-1–deficient synovial cells. These cells were derived from adult SOCS-1$^{-/-}$ mice established on an IFN-γ–null background to rescue the perinatal lethality associated with SOCS-1 deficiency (23). As revealed in Fig. 8 A, compound mutant SOCS-1$^{-/-}$, IFN-γ$^{-/-}$ cells, like gp130$^{\Delta STAT/\Delta STAT}$ cells, showed enhanced [^{3}H]thymidine incorporation in response to nanomolar concentrations of IL-6, compared with cells prepared from control mice of the corresponding genetic background (SOCS-1$^{+/+}$, IFN-γ$^{-/-}$, and gp130$^{\Delta STAT/wt}$, respectively). Compared with SOCS-1$^{+/+}$ IFN-γ$^{-/-}$ control cells, we also observed sustained IL-6–mediated Erk1/2 phosphorylation in SOCS-1$^{-/-}$ IFN-γ$^{-/-}$ cells (Fig. 8 B). Thus, the enhanced proliferative responsiveness to IL-6 was also a feature of SOCS-1$^{-/-}$ IFN-γ$^{-/-}$ cells, however, this was less marked than in gp130$^{\Delta STAT/\Delta STAT}$ cells.

If impaired or reduced induction of SOCS-1 (and SOCS-3) expression accounted for sustained activation of the Jak/SHP-2/ras/Erk cascade in response to IL-6 in gp130$^{\Delta STAT/\Delta STAT}$ synovial cells, then overexpression of SOCS-1 should revert the hyperresponsive phenotype of

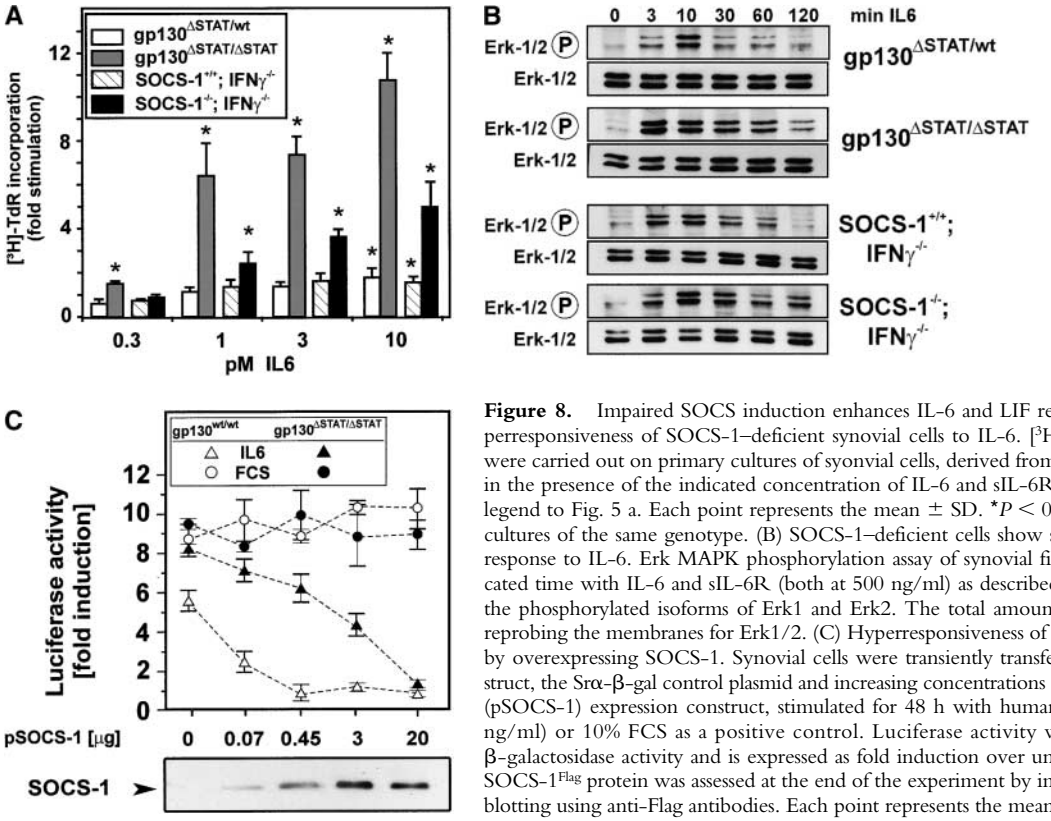

Figure 8. Impaired SOCS induction enhances IL-6 and LIF responsiveness. (A) Mitogenic hyperresponsiveness of SOCS-1–deficient synovial cells to IL-6. [^{3}H]thymidine incorporation assays were carried out on primary cultures of syonvial cells, derived from mice of the indicated genotype, in the presence of the indicated concentration of IL-6 and sIL-6R (500 ng/ml) as described in the legend to Fig. 5 a. Each point represents the mean ± SD. *$P < 0.05$ compared with unstimulated cultures of the same genotype. (B) SOCS-1–deficient cells show sustained activation of Erk1/2 in response to IL-6. Erk MAPK phosphorylation assay of synovial fibroblasts stimulated for the indicated time with IL-6 and sIL-6R (both at 500 ng/ml) as described in Fig. 5 b. Erk1/2-P indicates the phosphorylated isoforms of Erk1 and Erk2. The total amount of Erk protein was assessed by reprobing the membranes for Erk1/2. (C) Hyperresponsiveness of synovial cells to IL-6 is corrected by overexpressing SOCS-1. Synovial cells were transiently transfected with a *fos-luc* reporter construct, the Srα-β-gal control plasmid and increasing concentrations of a Flag-epitope tagged SOCS-1 (pSOCS-1) expression construct, stimulated for 48 h with human IL-6 plus sIL-6R (both at 500 ng/ml) or 10% FCS as a positive control. Luciferase activity was normalized by reference to β-galactosidase activity and is expressed as fold induction over unstimulated cultures. The level of SOCS-1^{Flag} protein was assessed at the end of the experiment by immunoprecipitation and Western blotting using anti-Flag antibodies. Each point represents the mean ± SD.

these cells. To explore this notion, we exploited the fact that the minimal *c-fos* promoter is activated through the ras/Erk pathway (27). As expected, IL-6 stimulation of gp130$^{\Delta STAT/\Delta STAT}$ cells, transiently transfected with a *c-fos*-luciferase reporter construct, yielded higher luciferase activity than IL-6 stimulation of wt cells (Fig. 8 C). Furthermore, increasing the cellular concentration of SOCS-1 protein, after cotransfection with an epitope tagged SOCS-1^{Flag} expression plasmid (pSOCS-1), reduced IL-6-responsiveness in gp130$^{\Delta STAT/\Delta STAT}$ cells to levels observed in wt cells. Finally, a complete block of IL-6–mediated luciferase activity in gp130$^{\Delta STAT/\Delta STAT}$ cells required greater amounts of transfected pSOCS-1 protein than in wt cells. Collectively, these observations are consistent with the notion that elevated levels of recombinant SOCS-1^{Flag} protein were required to terminate IL-6 signaling in gp130$^{\Delta STAT/\Delta STAT}$ mutant cells to compensate for impaired induction of endogenous SOCS-1 and SOCS-3 expression. Since recombinant SOCS-1^{Flag} expression did not suppress *c-fos*-luciferase activity induced by serum, overexpression of SOCS-1^{Flag} was not directly interfering with activity of the *c-fos*-luciferase reporter plasmid.

Taken together, these data strongly suggest that the hyperresponsiveness of synovial cells from gp130$^{\Delta STAT/\Delta STAT}$ mice arose from defective or impaired STAT-mediated SOCS induction which resulted in sustained activation of the SHP-2/ras/Erk pathway, leading to synovial hyperproliferation and cartilaginous metaplasia and ultimately the degeneration of the joint.

Discussion

At the molecular level, the multiple and tissue-specific activities of cytokines are explained, in part, by activation of multiple signaling cascades emanating from discrete intracellular receptor domains which regulate distinct (sets of) target genes. While complete inactivation of multidomain receptors will result in phenotypes reflecting inactivation of all associated signaling pathways, the selective deletion of one particular domain provides the opportunity to associate a specific signaling cascade with a particular physiological or pathological process. Here we used a knock-in strategy to mimic the effect of a nonsense mutation that specifically deletes the COOH-terminal domain of gp130, along with its associated STAT activation sites, but still permits activation of the SHP-2/ras/Erk pathway (15, 19). Consequently, the phenotype in gp130$^{\Delta STAT/\Delta STAT}$ mice is largely a direct consequence of the absence (in the case of gp130$^{\Delta STAT}$ homodimerization) or diminution (in the case of LIF-Rβ/gp130$^{\Delta STAT}$ heterodimerization) of STAT-mediated cellular responses. Furthermore, we also identified the importance of STAT signals in promoting inhibitory feedback signals on gp130 and the associated SHP-2/ras/Erk pathway, thereby reinforcing a concept that the two pathways are under reciprocal negative control (35).

The phenotypes of mice with gp130 impairment mutations affecting either the STAT (gp130$^{\Delta STAT/\Delta STAT}$ mice reported here) or the SHP-2/ras/Erk signaling cascade (gp130$^{757F/757F}$ mice; reference 35) are dramatically different from the myocardial hypoplasia and associated embry-

onic lethality observed in gp130$^{-/-}$ mice (11). Similarly, no profound effects on embryonic development were reported in gp130$^{FxxQ/FxxQ}$ mice, where STAT signaling was abolished after replacement of the cytoplasmic domain of gp130 with a human cDNA encoding phenylalanine substitutions in all YxxQ motifs (36). However, the latter mutation resulted in perinatal death associated with the apparent failure of milk uptake and perturbed CNTF-mediated astrocyte differentiation (35). Since the phenotype of gp130$^{FxxQ/FxxQ}$ mice is somewhat reminiscent of that observed in LIF-R$\beta^{-/-}$ (10) and CNTF-R$\alpha^{-/-}$ mice (36), but entirely different to that associated with IL-6$^{-/-}$ (4, 5) or IL-11Rα1$^{-/-}$ mice (8, 9), signaling through the heterodimeric LIF-Rβ/gp130 rather than through homodimeric gp130 appears critical after birth. Therefore, it is likely that STAT signaling through LIF-Rβ/gp130^{FxxQ} receptor heterodimers is rate limiting in gp130$^{FxxQ/FxxQ}$ mice, while signaling through LIF-Rβ/gp130$^{\Delta STAT}$ heterodimers, although decreased when compared with wt LIF-Rβ/gp130 dimers, reaches the threshold that enables postnatal survival of most of the gp130$^{\Delta STAT/\Delta STAT}$ pups. The "magnitude" of the STAT signal may be influenced by the rate of internalization of ligand occupied LIF-Rβ/gp130 complexes, which in turn is determined by the collective activity of individual dileucine internalization signals (L_{1064}I in LIF-Rβ and L_{984}L in gp130; references 37 and 38). Thus, one could speculate that LIF-Rβ/gp130^{FxxQ} dimers are more efficiently internalized than LIF-Rβ/gp130$^{\Delta STAT}$ dimers, and thus signal from the LIF-Rβ/gp130$^{\Delta STAT}$ dimers may be sustained for longer.

Degenerative Joint Disease in gp130$^{\Delta STAT/\Delta STAT}$ Mice. The most striking observation in gp130$^{\Delta STAT/\Delta STAT}$ mice was restricted joint movement which was apparent from an early age and consistently affected older mice albeit with variable severity. While early stages of the joint disease bear hallmarks of inflammation, the intermediate stages were reminiscent of rheumatoid arthritis with the overgrowing pannus-like tissue at the edge of the articular surface. Likewise, the formation of cartilage in these pannus-like tissues resembled osteoarthritis in which cartilaginous and osseous osteophytes formed along the rim of the eroded cartilage plate. The advanced stage with its overgrowth of cartilage along the synovial lining, however, resembled neither pathology but rather the rare human condition synovial chondromatosis (39), although the characteristic multiple "loose" bodies of hyaline cartilage within the joint space were only infrequently observed in gp130$^{\Delta STAT/\Delta STAT}$ mice.

Many studies have implicated the LIF/IL-6 family cytokines and their soluble receptors as proinflammatory mitogens for synovial fibroblasts in inflammatory joint diseases including rheumatoid arthritis (32, 33). Our model, in which signaling through gp130$^{\Delta STAT}$ resulted in impaired or reduced induction of SOCS-1 and SOCS-3, implicates activation of the SHP-2/ras/Erk pathway as the likely molecular mechanism promoting hyperproliferation of synovial cells by increasing their sensitivity to physiological levels of LIF/IL-6 cytokines. In turn, the hypersensitivity of these cells may trigger a sequence of changes including chronic synovitis that results in cartilaginous metaplasia and culminates in a degenerative process affecting the major weight-bearing joints. However, we cannot categorically exclude the possibility that synovial hyperplasia and the formation of exogenous cartilage occurred independently of each other.

Since our data provide strong genetic evidence for a critical involvement of gp130, STAT, and SOCS proteins in maintaining the integrity of joints of the appendicular skeleton, why do other mouse strains with mutations in either the LIF/IL-6 cytokine signaling cascade or in SOCS genes lack overt joint pathology? This apparent anomaly can be explained by extrapolating from observations by Ohtani et al. (35) who showed that the gp130-dependent STAT and SHP-2/ras/Erk pathways play reciprocal roles in the immune response by providing a balance between positive and negative signals. This delicate balance between the two pathways at the level of gp130 is further emphasized through their reciprocal negative regulation (35, 40, 41). Hence, balanced alterations of the signaling output from gp130-dependent STAT and SHP-2/ras/Erk pathways, either by attenuation (for instance in ligand and receptor null mutants) or augmentation (for instance in mice transgenic for the ligands), resulted in a number of phenotypes which were not observed in mice with an imbalance between the two pathways (for instance in gp130$^{\Delta STAT/\Delta STAT}$ or gp130$^{757F/757F}$ mice; reference 35). Similarly, the simultaneous and sustained activation of the SHP-2/ras/Erk and STAT pathways in response to IL-6 in synovial cells from SOCS-1$^{-/-}$ IFN-$\gamma^{-/-}$ compound mice did not result in cartilaginous overgrowth or destruction of the large weight-bearing joints. However, SOCS-1$^{-/-}$ IFN-$\gamma^{-/-}$ mice developed an acute synovitis of the tendons and small joints of distal limbs (unpublished data), presumably resulting from the activity of dysregulated T cells (42).

The gp130$^{\Delta STAT}$ Mutation Impairs Biological Responses to IL-6 and IL-11. Since IL-6 and IL-11 are the only cytokines that signal exclusively through gp130, we predicted that these cytokines would fail to elicit STAT-mediated responses in gp130$^{\Delta STAT/\Delta STAT}$ mice. This was clearly demonstrated by failure to induce type I acute phase proteins in the liver which is a STAT-mediated response in cultured hepatocytes (20). Furthermore, gp130$^{\Delta STAT/\Delta STAT}$ mice, like mice either deficient for IL-6 (4, 5, 30), or containing a conditional gp130-null allele (31), or mice transgenic for a truncated and dominant interfering gp130$^{\Delta 703}$ protein (43), displayed impairment of T cell–dependent high affinity immune and mucosal IgA responses. By contrast, constitutive activation of the STAT and the SHP-2/ras/Erk signaling cascades, as observed in IL-6 transgenic mice, resulted in IgG1 plasmacytosis (44), a phenotype that was never observed as a result of sustained activation of the SHP-2/ras/Erk pathway in gp130$^{\Delta STAT/\Delta STAT}$ mice. Collectively, these observations implicate STAT signaling, rather than activation of the SHP-2/ras/Erk pathway, as the driving force for IL-6–mediated plasma cell maturation.

Intriguingly, spontaneously occurring ulcerative lesions have not been previously observed as a consequence of the

genetic manipulation of the IL-6/LIF cytokine axis. Notably, no intestinal phenotype was observed in IL-$6^{-/-}$ or IL-$11R\alpha 1^{-/-}$ mice, although a role for STAT3 has been proposed during cell migration in epidermal wound healing (45). Thus, it is conceivable that intestinal ulceration in $gp130^{\Delta STAT/\Delta STAT}$ mice may result from a combination of STAT-dependent reduction in IL-6–mediated first line defense against pathogens at mucosal surfaces and impairment of epithelial homeostasis, which is maintained in the intestine, at least in part, through IL-11–mediated signaling (46).

The $gp130^{\Delta STAT}$ Mutation Reduces STAT Signaling from gp130/LIF-Rβ Complexes. The failure of blastocyst implantation in $gp130^{\Delta STAT/\Delta STAT}$ mice resembled in all aspects the defect observed in $LIF^{-/-}$ mice (6, 7) and suggests a pivotal role for the COOH-terminal region of gp130 and associated STAT signaling during blastocyst implantation and possibly decidua formation. Since STAT signaling from the mutant $gp130^{\Delta STAT}$/LIF-Rβ receptor heterodimer was compromised in all tissues examined, the implantation defect is the likely consequence of a failure to reach a threshold level of LIF-induced STAT signaling in the uterus of $gp130^{\Delta STAT/\Delta STAT}$ mice. However, we cannot exclude the possibility that the $gp130^{\Delta STAT}$ mutation may also affect the implantation capacity of the uterine epithelium in response to simultaneous stimulation by IL-6 and IL-11. Although blastocyst implantation in mice individually deficient for either IL-6 or IL-11 signaling was not affected (8, 9), increased IL-6 expression is observed in the epithelial cells of the endometrium during the "implantation window" (47). The generation of IL-$6^{-/-}$ IL-$11R\alpha^{-/-}$ mice will establish whether the simultaneous action of these two cytokines may play a hitherto unknown indispensable role during the process of uterine implantation.

This study genetically implicates gp130-mediated STAT signaling in a number of physiological host responses affecting uterine implantation, type I acute phase response, humoral and mucosal immune response, and epithelial homeostasis in the gastrointestinal tract. Surprisingly, blunting of STAT signaling in the joint compartment resulted in the mitogenic hyperresponsiveness of the synovial cells thereby triggering a series of pathological responses which ultimately culminated in the degeneration of the joints. This observation is consistent with a requirement for the balanced activation of the SHP-2/ras/Erk and STAT pathways to maintain synovial homeostasis in response to gp130 signaling and highlights the crucial role for the LIF/IL-6 cytokine family in retaining the integrity of joint architecture and function. To date, no disorder has been associated with impaired gp130 signaling in humans, however, germline mutations yielding a premature stop codon have been found in the related receptor for granulocyte colony stimulating factor in a subset of patients with severe congenital neutropenia (48). On the assumption that gp130 truncation mutations in humans would phenocopy at least some of the abnormalities observed in $gp130^{\Delta STAT}$ mice, one might speculate that a subset of patients with degenerative joint diseases, female infertility, or impaired mucosal immunity may result from nonsense mutations in gp130 or other genetic lesions that impair gp130-mediated STAT signaling.

We are grateful to Drs. Richard Simpson for providing IL-6 and sIL-6R and Robyn Starr for making available the pSOCS-1 expression construct. Dr. Lorraine Robb is thanked for advice on embryo implantation, Dianne Grail for expert animal husbandry, Val Feakes for histological support, and Janna Stickland for photography.

Submitted: 25 September 2000
Revised: 31 May 2001
Accepted: 12 June 2001

References

1. Heinrich, P.C., I. Behrmann, G. Muller-Newen, F. Schaper, and L. Graeve. 1998. Interleukin-6-type cytokine signaling through the gp130/Jak/STAT pathway. *Biochem. J.* 334:297–314.
2. Taga, T., and T. Kishimoto. 1997. Gp130 and the interleukin-6 family of cytokines. *Annu. Rev. Immunol.* 15:797–819.
3. Waring, P. 1997. Leukemia inhibitory factor. *In* Colony Stimulating Factors, Molecular and Cellular Biology. Second ed. J.M. Garland, editor. Marcel Dekker Publishers, New York. 467–513.
4. Kopf, M., H. Baumann, G. Freer, M. Freudenberg, M. Lamers, T. Kishimoto, R. Zinkernagel, H. Bluethmann, and G. Kohler. 1994. Impaired immune and acute-phase responses in interleukin-6-deficient mice. *Nature.* 368:339–342.
5. Ramsay, A.J., A.J. Husband, I.A. Ramshaw, S. Bao, K.I. Matthaei, G. Koehler, and M. Kopf. 1994. The role of interleukin-6 in mucosal IgA antibody responses in vivo. *Science.* 264:561–563.
6. Stewart, C.L., P. Kaspar, L.J. Brunet, H. Bhatt, I. Gadi, F. Kontgen, and S.J. Abbondanzo. 1992. Blastocyst implantation depends on maternal expression of leukaemia inhibitory factor. *Nature.* 359:76–79.
7. Escary, J.L., J. Perreau, D. Dumenil, S. Ezine, and P. Brulet. 1993. Leukaemia inhibitory factor is necessary for maintenance of haematopoietic stem cells and thymocyte stimulation. *Nature.* 363:361–364.
8. Robb, L., R. Li, L. Hartley, H.H. Nandurkar, F. Koentgen, and C.G. Begley. 1998. Infertility in female mice lacking the receptor for interleukin 11 is due to a defective uterine response to implantation. *Nat. Med.* 4:303–308.
9. Bilinski, P., D. Roopenian, and A. Gossler. 1998. Maternal IL-11R-α function is required for normal decidua and fetoplacental development in mice. *Genes Dev.* 12:2234–2243.
10. Ware, C.B., M.C. Horowitz, B.R. Renshaw, J.S. Hunt, D. Liggitt, S.A. Koblar, B.C. Gliniak, H.J. McKenna, T. Papayannopoulou, B. Thoma, et al. 1995. Targeted disruption of the low-affinity leukemia inhibitory factor receptor gene causes placental, skeletal, neural and metabolic defects and results in perinatal death. *Development.* 121:1283–1299.
11. Yoshida, K., T. Taga, M. Saito, S. Suematsu, A. Kumanogoh, T. Tanaka, H. Fujiwara, M. Hirata, T. Yamagami, T. Nakahata, et al. 1996. Targeted disruption of gp130, a common signal transducer for the interleukin 6 family of cytokines, leads to myocardial and hematological disorders. *Proc. Natl. Acad. Sci. USA.* 93:407–411.
12. Kawasaki, K., Y.H. Gao, S. Yokose, Y. Kaji, T. Nakamura, T. Suda, K. Yoshida, T. Taga, T. Kishimoto, H. Kataoka, et al. 1997. Osteoclasts are present in gp130-deficient mice. *En-*

docrinology. 138:4959–4965.
13. Saito, M., K. Yoshida, M. Hibi, T. Taga, and T. Kishimoto. 1992. Molecular cloning of a murine IL-6 receptor-associated signal transducer, gp130, and its regulated expression in vivo. *J. Immunol.* 148:4066–4071.
14. Tomida, M., Y. Yamamoto-Yamaguchi, and M. Hozumi. 1994. Three different cDNAs encoding mouse D-factor/LIF receptor. *J. Biochem.* 115:557–562.
15. Fukada, T., M. Hibi, Y. Yamanaka, M. Takahashi-Tezuka, Y. Fujitani, T. Yamaguchi, K. Nakajima, and T. Hirano. 1996. Two signals are necessary for cell proliferation induced by a cytokine receptor gp130: involvement of STAT3 in anti-apoptosis. *Immunity*. 5:449–460.
16. Stahl, N., T.J. Farruggella, T.G. Boulton, Z. Zhong, J.E. Darnell, Jr., and G.D. Yancopoulos. 1995. Choice of STATs and other substrates specified by modular tyrosine-based motifs in cytokine receptors. *Science*. 267:1349–1353.
17. Yamanaka, Y., K. Nakajima, T. Fukada, M. Hibi, and T. Hirano. 1996. Differentiation and growth arrest signals are generated through the cytoplasmic region of gp130 that is essential for Stat3 activation. *EMBO J.* 15:1557–1565.
18. Niwa, H., T. Burdon, I. Chambers, and A. Smith. 1998. Self-renewal of pluripotent embryonic stem cells is mediated via activation of STAT3. *Genes Dev.* 12:2048–2060.
19. Ernst, M., U. Novak, S.E. Nicholson, J.E. Layton, and A.R. Dunn. 1999. The carboxyl-terminal domains of gp130-related cytokine receptors are necessary for suppressing embryonic stem cell differentiation: involvement of STAT3. *J. Biol. Chem.* 274:9729–9737.
20. Lai, C.F., J. Ripperger, Y. Wang, H. Kim, R.B. Hawley, and H. Baumann. 1999. The STAT3-independent signaling pathway by glycoprotein 130 in hepatic cells. *J. Biol. Chem.* 274:7793–7802.
21. Starr, R., T.A. Willson, E.M. Viney, L.J. Murray, J.R. Rayner, B.J. Jenkins, T.J. Gonda, W.S. Alexander, D. Metcalf, N.A. Nicola, and D.J. Hilton. 1997. A family of cytokine-inducible inhibitors of signaling. *Nature*. 387:917–921.
22. Naka, T., M. Narazaki, M. Hirata, T. Matsumoto, S. Minamoto, A. Aono, N. Nishimoto, T. Kajita, T. Taga, K. Yoshizaki, et al. 1997. Structure and function of a new STAT-induced STAT inhibitor. *Nature*. 387:924–929.
23. Alexander, W.S., R. Starr, J.E. Fenner, C.L. Scott, E. Handman, N.S. Sprigg, J.E. Corbin, A.L. Cornish, R. Darwiche, C.M. Owczarek, et al. 1999. SOCS1 is a critical inhibitor of interferon γ signaling and prevents the potentially fatal neonatal actions of this cytokine. *Cell*. 98:597–608.
24. Dalton, D.K., S. Pitts-Meek, S. Keshav, I.S. Figari, A. Bradley, and T.A. Stewart. 1993. Multiple defects of immune cell function in mice with disrupted interferon-γ genes. *Science*. 259:1739–1742.
25. Crofford, L.J., R.L. Wilder, A.P. Ristimaki, H. Sano, E.F. Remmers, H.R. Epps, and T. Hla. 1994. Cyclooxygenase-1 and –2 expression in rheumatoid synovial tissues; effects of interleukin-1β, phorbol ester and corticosteroids. *J. Clin. Invest.* 93:1095–1101.
26. Lambert, N., P.L. Lescoulie, B. Yassine-Diab, G. Enault, B. Mazieres, C. De Preval, and A. Cantagrel. 1998. Substance *P* enhances cytokine-induced vascular cell adhesion molecule-1 (VCAM-1) expression on cultured rheumatoid fibroblast-like synoviocytes. *Clin. Exp. Immunol.* 113:269–275.
27. Watanabe, S., A.L. Mui, A. Muto, J.X. Chen, K. Hayashida, T. Yokota, A. Miyajima, and K. Arai, K. 1993. Reconstituted human granulocyte-macrophage colony-stimulating factor receptor transduces growth-promoting signals in mouse NIH 3T3 cells: comparison with signaling in BA/F3 pro-B cells. *Mol. Cell. Biol.* 13:1440–1448.
28. Nicholson, S.E., T.A. Willson, A. Farley, R. Starr, J.G. Zhang, M. Baca, W.S. Alexander, D. Metcalf, D.J. Hilton, and N.A. Nicola. 1999. Mutational analyses of the SOCS proteins suggest a dual domain requirement but distinct mechanisms for inhibition of LIF and IL-6 signal transduction. *EMBO J.* 18:375–385.
29. Campbell, I.K., S. Gerondakis, K. O'Donnell, and I.P. Wicks. 2000. Distinct roles for the NF-kappaB1 (p50) and c-Rel transcription factors in inflammatory arthritis. *J. Clin. Invest.* 105:1799–1806.
30. Bao, S., A.J. Husband, and K.W. Beagley. 1999. B1 B cell numbers and antibodies against phosphorylcholine and LPS are increased in IL-6 gene knockout mice. *Cell. Immunol.* 198:139–142.
31. Betz, U.A.K., W. Bloch, M. van den Broek, K. Yoshida, T. Taga, T. Kishimoto, K. Addicks, K. Rajewsky, and W. Muller. 1998. Postnatally induced inactivation of gp130 in mice results in neurological, cardiac, hematopoietic, immunological, hepatic, and pulmonary defects. *J. Exp. Med.* 188: 1955–1965.
32. Mihara, M., Y. Moriya, T. Kishimoto, and Y. Ohsugi. 1995. Interleukin-6 (IL-6) induces the proliferation of synovial fibroblastic cells in the presence of soluble IL-6 receptor. *Br. J. Rheumatol.* 34:321–325.
33. Waring, P.M., G.J. Carroll, D.A. Kandiah, G. Buirski, and D. Metcalf. 1993. Increased levels of leukemia inhibitory factor in synovial fluid from patients with rheumatoid arthritis and other inflammatory arthritides. *Arthritis. Rheum.* 36:911–915.
34. Bousquet, C., C. Sisini, and S. Melmed. 1999. Inhibitory roles for SHP-1 and SOCS-3 following pituitary pro-opiomelanocortin induction by leukemia inhibitory factor. *J. Clin. Invest.* 104:1277–1285.
35. Ohtani, T., K. Ishihara, T. Atsumi, K. Nishida, Y. Kaneko, T. Miyata, S. Itoh, M. Narimatsu, H. Maeda, T. Fukada, et al. 2000. Dissection of signal cascades through gp130 in vivo: reciprocal roles for STAT3 and SHP2-mediated signals in immune responses. *Immunity*. 12:95–105.
36. DeChiara, T.M., R. Vejsada, W.T. Poueymirou, A. Acheson, C. Suri, J.C. Conover, B. Friedman, J. McClain, L. Pan, N. Stahl, et al. 1995. Mice lacking the CNTF receptor, unlike mice lacking CNTF, exhibit profound motor neuron deficits at birth. *Cell*. 83:313–322.
37. Thiel, S., I. Behrmann, A. Timmermann, H. Dahmen, G. Muller-Newen, F. Schaper, J. Tavernier, V. Pitard, P.C. Heinrich, and L. Graeve. 1999. Identification of a Leu-lle internalization motif within the cytoplasmic domain of the leukaemia inhibitory factor receptor. *Biochem. J.* 339:15–19.
38. Dittrich, E., C.R. Haft, L. Muys, P.C. Heinrich, and L. Graeve. 1996. A di-leucine motif and an upstream serine in the interleukin-6 (IL-6) signal transducer gp130 mediate ligand-induced endocytosis and down-regulation of the IL-6 receptor. *J. Biol. Chem.* 271:5487–5494.
39. Rosenberg, A.E., and A.L. Schiller. 1993. Tumors and tumor-like lesions of joints. *In* Textbook of Rheumatology. Vol. 2, fourth ed. W.N. Kelley, E.D. Harris, S. Ruddy, and C.B. Sledge, editors. W.B. Saunders Company, Philadelphia. 1656–1660.
40. Nicholson, S.E., D. De Souza, L.J. Fabri, J. Corbin, T.A. Willson, J.G. Zhang, A. Silva, M. Asimakis, A. Farley, A.D.

Nash, et al. 2000. Suppressor of cytokine signaling-3 preferentially binds to the SHP-2-binding site on the shared cytokine receptor subunit gp130. *Proc. Natl. Acad. Sci. USA*. 97: 6493–6498.

41. Fukada, T., Y. Yoshida, K. Nishida, T. Othani, T. Shirogane, M. Hibi, and T. Hirano 2000. Signaling through gp130: towards a general scenario of cytokine action. *Growth Factors*. 17:81–91.
42. Fujimoto, M., T. Naka, R. Nakagawa, Y. Kawazoe, Y. Morita, A. Tateishi, K. Okumura, M. Narazaki, and T. Kishimoto. 2000. Defective thymocyte development and perturbed homeostasis of T cells in STAT-induced STAT inhibitor-1/suppressors of cytokine signaling-1 transgenic mice. *J. Immunol*. 165:1799–1806.
43. Kumanogoh, A., S. Marukawa, T. Kumanogoh, H. Hirota, K. Yoshida, I.S. Lee, T. Yasui, K. Yoshida, T. Taga, and T. Kishimoto. 1997. Impairment of antigen-specific antibody production in transgenic mice expressing a dominant-negative form of gp130. *Proc. Natl. Acad. Sci. USA*. 94:2478–2482.
44. Suematsu, S., T. Matsuda, K. Aozasa, S. Akira, N. Nakano, S. Ohno, J. Miyazaki, K. Yamamura, T. Hirano, and T. Kishimoto. 1989. IgG1 plasmacytosis in interleukin 6 transgenic mice. *Proc. Natl. Acad. Sci. USA*. 86:7547–7551.
45. Sano, S., S. Itami, K. Takeda, M. Tarutani, Y. Yamaguchi, H. Miura, K. Yoshikawa, S. Akira, and J. Takeda. 1999. Keratinocyte-specific ablation of Stat3 exhibits impaired skin remodeling, but does not affect skin morphogenesis. *EMBO J*. 18:4657–4668.
46. Du, X., and D.A. Williams. 1997. Interleukin-11: review of molecular, cell biology, and clinical use. *Blood*. 89:3897–3908.
47. Liang, L., K. Kover, S.K. Dey, and G.K. Andrews. 1996. Regulation of interleukin-6 and interleukin-1β gene expression in the mouse deciduum. *J. Reprod. Immunol*. 30:29–52.
48. Dong, F., L.H. Hoefsloot, A.M. Schelen, C.A. Broeders, Y. Meijer, A.J. Veerman, I.P. Touw, and B. Lowenberg. 1994. Identification of a nonsense mutation in the granulocyte-colony-stimulating factor receptor in severe congenital neutropenia. *Proc. Natl. Acad. Sci. USA*. 91:4480–4484.